Supporting Information

Gonzalez-Bellido et al. 10.1073/pnas.1210489109

SI Materials and Methods

Animals. Adult *Libellula luctuosa* were netted outside the Howard Hughes Medical Institute Janelia Farm Research Campus between March and August of 2011. Animals were immobilized with a metal jacket. Wax was used to further restrict animal movement. A small opening was made between the prothoracic and mesothoracic legs, and a metal support was placed underneath the ventral nerve cord [for a diagram, see Adelman et al. (1)]. The ventral nerve cord was impaled between the prothoracic and mesothoracic ganglia with borosilicate electrodes (Sutter; 10 cm; o.d., 1; i.d., 0.5; #BF-100-50-10; pulled with a Sutter P2000) filled with 1.5% Lucifer Yellow (Invitrogen; #L-453) in 100 mM LiCl and backfilled with 1 M LiCl (100-180 MΩ). The intracellular signal was amplified (Axoclamp; Axon Instruments), digitized (40 kHz), displayed, and recorded (Spike GL; A. Leonardo, Janelia Farm Research Campus, Ashburn, VA) for off-line analysis, which was carried out in MATLAB.

Stimulus. The animal was supported ventral-side-up by a clamp and the head tilted so that the dorsal area of the eye looked at the backprojected screen (see Fig. S6 for more details). Custom-written software (A. Leonardo) controlled the display of an image. The stimuli output were rendered by a graphics card with two display ports. Each display port was connected to a customized DLP projector (Light Speed; model: DepthQ) running at 360 Hz. The projectors were aligned without a gap between the images and the stimuli backprojected on a single piece of paper to create a continuous screen. This arrangement allowed stimuli to run seamlessly between the two displays. The full screen size (in pixels) was 1,600 wide by 600 high, placed 12 cm away from the head of the animal. The image projection size was 12.8 cm (height) × 33 cm (width). Therefore, the subtended screen size was 108° wide by 56° high. The target diameter subtended 1.48° (0.45 cm, 22 pixels), and the distance between target locations within a trajectory was 0.43° (0.13212 mm, 6.4 pixels). Hence, the targets between two consecutive locations overlapped by two-thirds of the target size. This assured that the target was seen as an object in continuous motion. A second signal from a photodiode monitoring the screen frame rate and timing was also recorded, allowing synchronization of the recording with the stimulus.

Electrophysiological Data Analysis. Target-selective descending neurons (TSDNs) were recognized initially by the following properties: robust responses to small moving targets of fixed size, increased response for certain target directions (i.e., directional selectivity), and lack of responses to a wide-field stimulus (such as a black-and-white grating in any orientation and direction). The data from cells impaled in the left connective were flipped along the midsagittal plane, so all responses are shown for the TSDNs in the right connective.

Latency Calculation. We obtained the minimum latency between stimulus onset/offset and cell first/last responses by creating a peristimulus histogram of spike timing for each recording (Fig. S1). The data were smoothed with an adjacent average weighted filter (3 ms). The second derivative of the smoothed trace was calculated. The time from movement onset to the first local maximum of the second derivative (corresponding to the moving target response) was taken as the latency. To avoid mistaking noise for spikes, the second derivative and the smoothed trace were plotted together. Visual inspection confirmed that the local maxima of the second derivative corresponded to the start of the responses to a moving target, and not to background spiking. The same procedure was carried out for the last responses.

Directional Tuning Calculation. For every spike recorded, the direction of the moving target that elicited it was noted. The data were grouped in 10° bins and plotted in polar form (Fig. 2*A*). Note that the spikes due to the "flash" response caused by the appearing target were not taken into account. The preferred cell direction (Fig. 2*A*, red dot) was obtained by using the CircStat MATLAB toolbox developed by Berens (2), which fits a Gaussian to the direction preference distribution of each cell. To obtain the tuning width of each cell accurately, the MATLAB toolbox published by Cronin et al. (3) was used. This toolbox uses a Bayesian method to estimate the tuning parameters.

Receptive Field Calculation. The onset latency obtained for each cell was used to calculate the target locations that elicited each spike. The average direction of the targets was calculated for each pixel [Fig. 2, direction receptive field (DRF) plots]. In addition, the spike-triggered average (STA) was calculated to yield the receptive fields shown in Fig. 2 (STA plots). Note that, in DRF plots, a pixel with a single spike is always marked with a bright color, because color denotes direction. However, in the STA maps, only the pixels with proportionally larger number of spikes look bright, because brightness codes number of spikes.

Looming Sensitivity. *L. luctuosa* TSDNs were tested with a linearly looming stimuli. The linear looming stimulus presented consisted of a target that grew in diameter from 1.35 to 31.86° in 158 ms and was presented in three different locations of the screen (left, center, and right) consecutively (Fig. S4*B*). Thus, the rate of diameter expansion was 19° per 100 ms. For comparative purposes, the reference system for the three locations of the expanding stimulus has been changed to ipsilateral, center, and contralateral. For example, an expanding stimulus was ipsilateral if it was presented on the right side of the screen and the cell was impaled in the right side of the connective. We counted the number of spikes elicited by each stimulus expansion. The mean spike number and the SE were calculated for each type of TSDN. In addition, *Libellula pulchella* TSDNs were tested with an angular expansion (1 m/s) of a 1-cm target.

Recording Temperature. Caution should be used when interpreting the electrophysiological results from this study. The animal and the room temperature were set at 23–25 °C during the recordings. Although this is above 19 °C, the minimum flying temperature in a Libellulid species, it is drastically lower than the Libellulid body temperature measured in specimens that were flying at the time of capture (28–36 °C) (4).

Recording Duration and STA Maps. Of the total number of intracellular recordings, 17 did not complete the full sequence of trajectories (only four records had less than 2,500 trajectories and none of those were below 1,500 trajectories). Although a lower number of presented trajectories also lowered the total number of recorded spikes, it did not affect the direction or receptive field results (Fig. S5). The spikes from each recording were used to create the STA (Fig. S5). All of the STAs from the same type of

TSDNs were normalized, averaged, and normalized again, shown as STA maps in Fig. 2.

Population Vector Computation. In some trials, the target position presented a "wrapping" effect as they hit the edge of the screen. The 2,776 trajectories that did not exhibit target wrapping were used to compute the population vectors.

In the ensuing part, the raw electrophysiology data were reanalyzed. This time, target directions were binned every 18°, cell activity was averaged per bin, and preferred directions were recalculated from these binned data. To obtain the cell activity for each target presented, we used the following bootstrap method. In a single bootstrap, a new sample of $n = 2{,}776$ target motion directions was formed for each cell by resampling with replacement the existing 2,776 trials, and so on for 100 bootstraps.

To calculate a population vector from the activity of a neural ensemble, it is first necessary to obtain a tuning curve function that describes the directional properties of each cell. A tuning curve function with a good fit yields the cell's activity $d(\theta)$ in response to a particular stimulus θ. For example, Eq. **S1** is a suitable tuning function when the frequency discharge of a cell is sinusoidal and depends on stimulus direction (5) as follows:

$$d(\theta) = b_0 + b_1 \sin\theta + b_2 \cos\theta + e, \qquad \textbf{[S1]}$$

where $d(\theta)$ is the rate of cell activity, b_0, b_1, b_2 are regression coefficients, and e is an error term.

For TSDNs, we have found that, in addition to the main bell-shaped cell activity curve, the cells also display a second smaller peak. This is taken into account by Eq. **S2** as follows:

$$d(\theta) = b_0 + b_1 \sin\theta + b_2 \cos\theta + b_3 \sin 2\theta + b_4 \cos 2\theta + e. \qquad \textbf{[S2]}$$

We confirmed the good fit of this function by calculating the multiple correlation coefficients R. This function yielded highly statistically significant fits ($P < 0.01$; $P < 0.001$ for 47 of 50 cells) and high R^2 (range: 0.65–0.978; mean, 0.918; median, 0.938). Such a good fit allows us to estimate correctly the preferred direction of the cell (θ_o), given by Eq. **S3** (5) as follows:

$$\theta_0 = tan^{-1}\frac{b_1}{b_2}. \qquad \textbf{[S3]}$$

Before calculating the population vector, the activity of each ith cell for stimulus θ, $C_i(\theta)$, was weighted using Eq. **S4**, shown as weight 12 in appendix 1 of ref. 6, as follows:

$$w_{i\theta} = \frac{d(\theta) - b_0}{b_0}. \qquad \textbf{[S4]}$$

Finally, the population vector for each target presented, $P(\theta)$, was calculated by summing weighted vectorial contributions from each of N cells in the population (6) as follows:

$$P(\theta) = \sum_{i}^{N} w_{i\theta} \cdot \theta_0. \qquad \textbf{[S5]}$$

Within the mesothoracic and metathoracic ganglia, the vast majority of motor neurons are ipsilateral. Therefore, the information is not likely to cross over from one side of the ganglia to the other side. For this reason and in absence of additional information, it is parsimonious to assume that the movement of each wing can only be formed by a population vector arising from the inputs into that specific side of the ganglia. Due to the receptive field location and to the anatomy of the TSDNs, a target moving in the left side of the visual field generates a different set of inputs for each side of the ganglia. This is to say that the population vector of the right and left wings arise from different sets of TSDNs inputs. This is the reason behind dividing TSDNs into groups that form right and left population vectors.

Correlation coefficients for circular data were calculated as shown by ref. 7.

For a graphical explanation of population vector coding, see Fig. S9.

Dye Injection, Sample Processing, and Confocal Imaging. Following electrophysiological characterization, the injection period was typically between 30 min and 2 h. To visualize injection of the dye, a Kramer quad illumination system with an X-cite fluorescence light source was used. Immunohistochemistry and streptavidin binding were used to tag the injected Lucifer yellow with DyLight 633, shifting the signal to the red spectrum. Each sample was imaged with three different channels; the background fluorescence, the trachea fluorescence, and the injected dye signal (Fig. S7). The first two were used to place landmarks for warping.

Image Reconstruction, Warping, and Tracing. To visualize the cell morphology, Vaa3D software was used (www.vaa3d.org) (8). The Vaa3D-iStitch plug in was used to stitch the images (9). To register the images, one sample was used as a model, and all subsequent samples were registered based on 48 markers manually determined using Vaa3D. The BrainAligner tool (10) was used to warp all samples to the model. To obtain the morphology of these cells, we developed a neuron-tracing method based on distance-transform of images.

1. Adelman TL, Bialek W, Olberg RM (2003) The information content of receptive fields. *Neuron* 40(4):823–833.
2. Berens P (2009) CircStat: A MATLAB toolbox for circular statistics. *J Stat Softw* 31(10): 1–21.
3. Cronin B, Stevenson IH, Sur M, Körding KP (2010) Hierarchical Bayesian modeling and Markov chain Monte Carlo sampling for tuning-curve analysis. *J Neurophysiol* 103(1): 591–602.
4. May ML (1976) Thermoregulation and adaptation to temperature in dragonflies (Odonata: Anisoptera). *Ecol Monogr* 46(1):1–32.
5. Georgopoulos AP, Kalaska JF, Caminiti R, Massey JT (1982) On the relations between the direction of two-dimensional arm movements and cell discharge in primate motor cortex. *J Neurosci* 2(11):1527–1537.
6. Georgopoulos AP, Kettner RE, Schwartz AB (1988) Primate motor cortex and free arm movements to visual targets in three-dimensional space. II. Coding of the direction of movement by a neuronal population. *J Neurosci* 8(8):2928–2937.
7. Fisher NI, Lee AJ (1983) A correlation coefficient for circular data. *Biometrika* 70(2):327–332.
8. Peng H, Ruan Z, Long F, Simpson JH, Myers EW (2010) V3D enables real-time 3D visualization and quantitative analysis of large-scale biological image data sets. *Nat Biotechnol* 28(4):348–353.
9. Yu Y, Peng H (2011) Automated high speed stitching of large 3D microscopic images. *Biomedical Imaging: From Nano to Macro, 2011 IEEE International Symposium* (IEEE, Chicago, IL), pp 238–241.
10. Peng H, et al. (2011) BrainAligner: 3D registration atlases of Drosophila brains. *Nat Methods* 8(6):493–500.

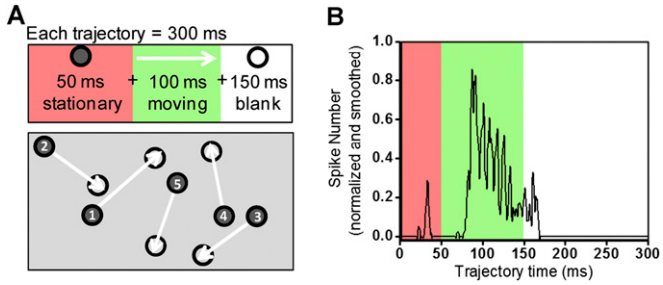

Fig. S1. Visual stimulus. (*A*) Each presented trajectory was composed of a target (1.48°, solid black circle on white background) that appeared in a random location and waited for 50 ms before moving for 100 ms and traveling 13.4° (4.1 cm) along a straight path in a random direction with a constant speed of 134°/s (41 cm/s). The target then disappeared for 150 ms before appearing again. The same random sequence was presented to all impaled cells. (*B*) We created a peristimulus histogram of spike timing for each recording (only one shown). This histogram provided the minimum latency between stimulus onset/offset and cell first/last responses.

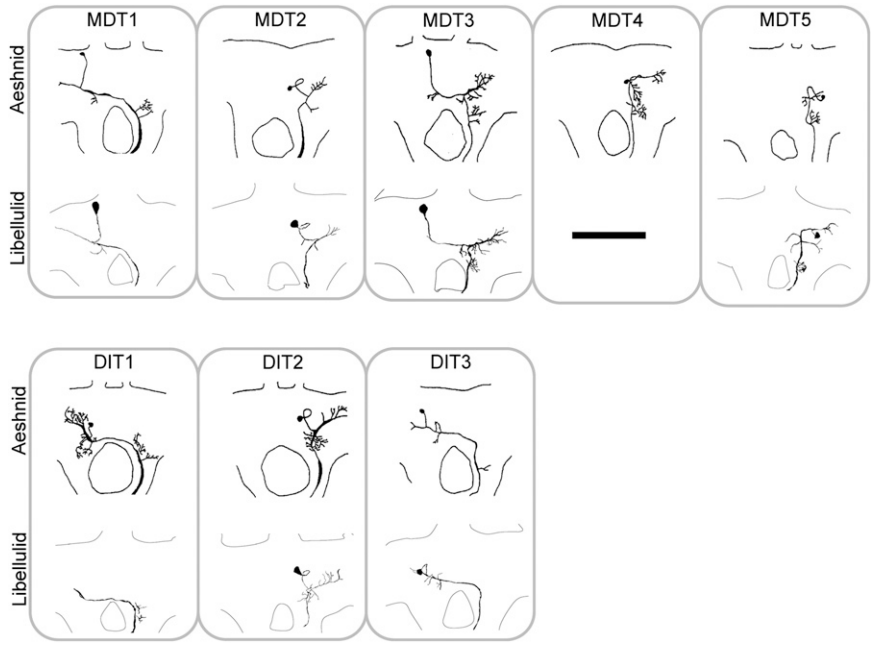

Fig. S2. The traces of TSDNs* from brains of the hawker dragonfly *Anax junius* (Aeshnid) and the percher dragonfly *L. luctuosa* (Libellulid) show homology. (Only TSDNs to the right of the midsagittal plane are shown. Trace for MDT4 is not available. The trace for DIT1 does not display a cell body due to an incomplete fill.) Traces were acquired from maximum-intensity projections of the brains. Aeshnid data were reproduced from Frye and Olberg (1).

1. Frye MA, Olberg RM (1995) Visual receptive-field properties of feature detecting neurons in the dragonfly. *J Comp Physiol A Neuroethol Sens Neural Behav Physiol* 177(5):569–576.

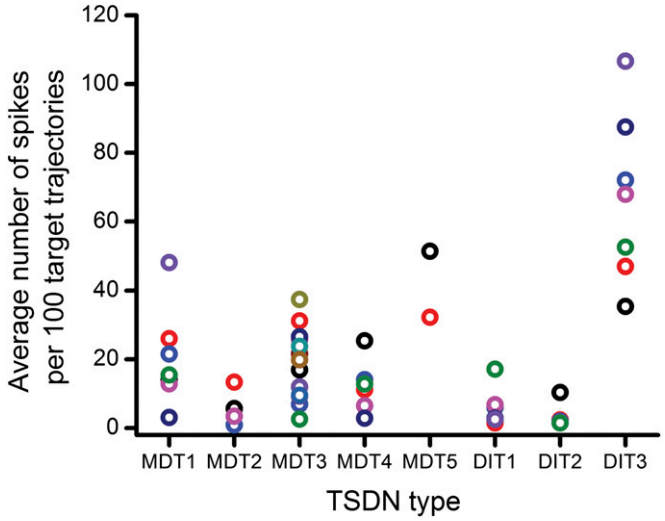

Fig. S3. Number of spikes recorded for each TSDN type differs among animals. This variation in number of spikes is not likely to be due to recording quality because we have observed recordings with large spikes, stable over prolonged periods but few in number. Although we have found that poor animal health is correlated with a low success in recording TSDNs for prolonged periods, we have also observed strong healthy animals responding with low number of spikes. Thus, on its own, animal health cannot explain spike number variance. It is most likely that the variance in spike numbers arise from differences in the state of the animal. In addition, because these animals are immobilized for the experiment, the lack of appropriate movement and feedback signals may impact some specimens more strongly.

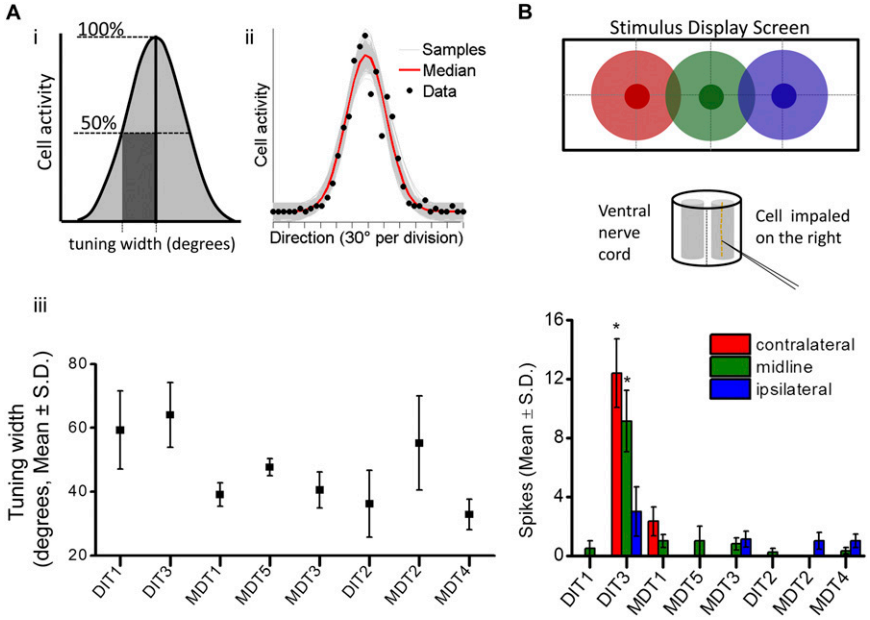

Fig. S4. TSDNs tuning width and looming sensitivity. (*A*) The tuning width of the TSDNs tuning curves, i.e., one-half the maximum width at one-half the maximum height (*i*), were calculated using the MATLAB toolbox published by Cronin et al. (1). This toolbox uses a Bayesian method to fit the data and estimate the tuning parameters. (*ii*) Analysis output example showing data points (grouped into 10° bins) from one MDT1 cell (black dots), mean fit (red), and the posterior samples (gray). (*iii*) The results show that the tuning widths varied significantly between TSDN types. (*B*) A linearly expanding stimulus consisting of a target which grew in diameter from 1.35 to 31.86° in 158 ms was presented in three different locations of the screen. This expanding stimulus only elicited a significant number of spikes at the contralateral ($P = 0.006$, $n = 5$) and midline ($P = 0.004$, $n = 7$) locations of DIT3 (asterisk). One-sample *t* test was used to test statistical significance.

1. Cronin B, Stevenson IH, Sur M, Körding KP (2010) Hierarchical Bayesian modeling and Markov chain Monte Carlo sampling for tuning-curve analysis. *J Neurophysiol* 103(1):591–602.

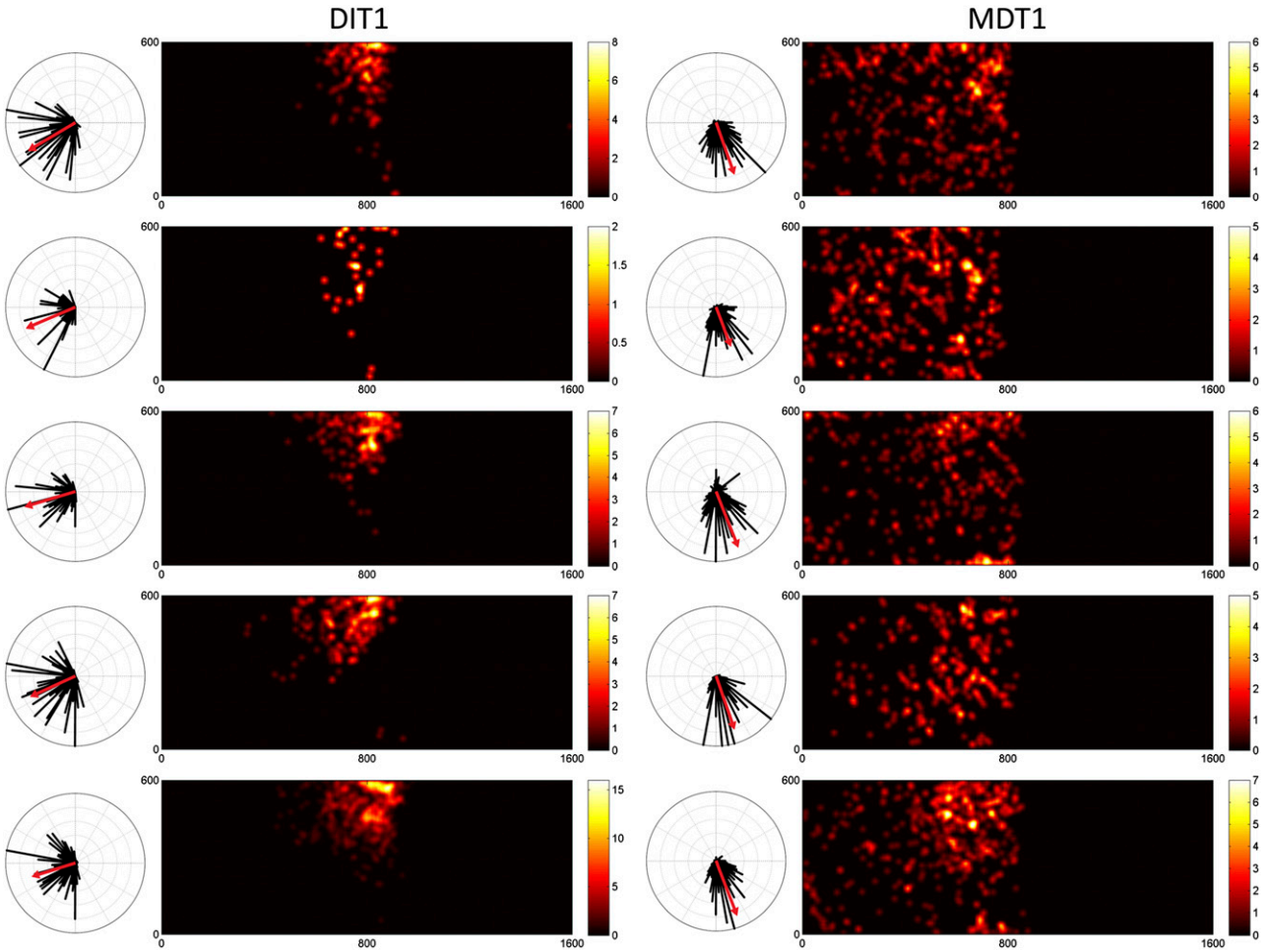

Fig. S5. For two TSDN types, DIT1 and MDT1, the characteristics of five of the contributing cells are shown. Number of spikes are plotted according to the direction of the target that elicited them (polar plot) and to the location where the target was, after taking into account the appropriate latency (spike-triggered average map). The receptive fields and direction preferences of the cells are constant across specimens, but their spike numbers are not. The scale for each STA notes the number of spikes at each pixel.

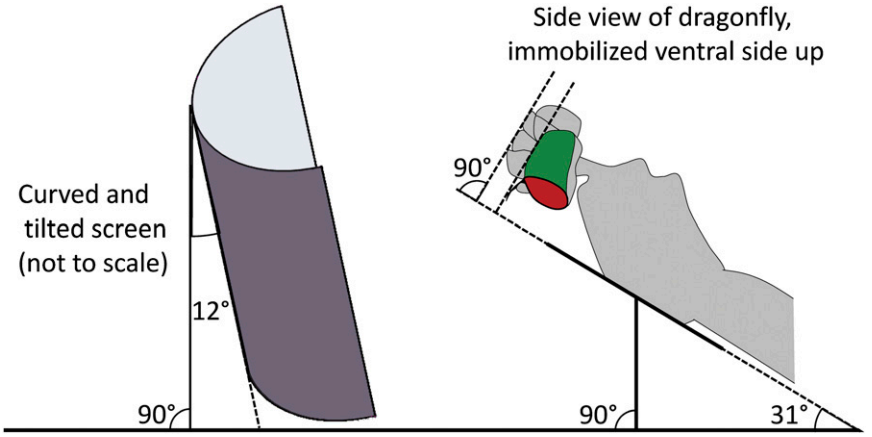

Fig. S6. The dragonfly was immobilized, with the eye pointing at the backprojected screen with the angles shown in the graph.

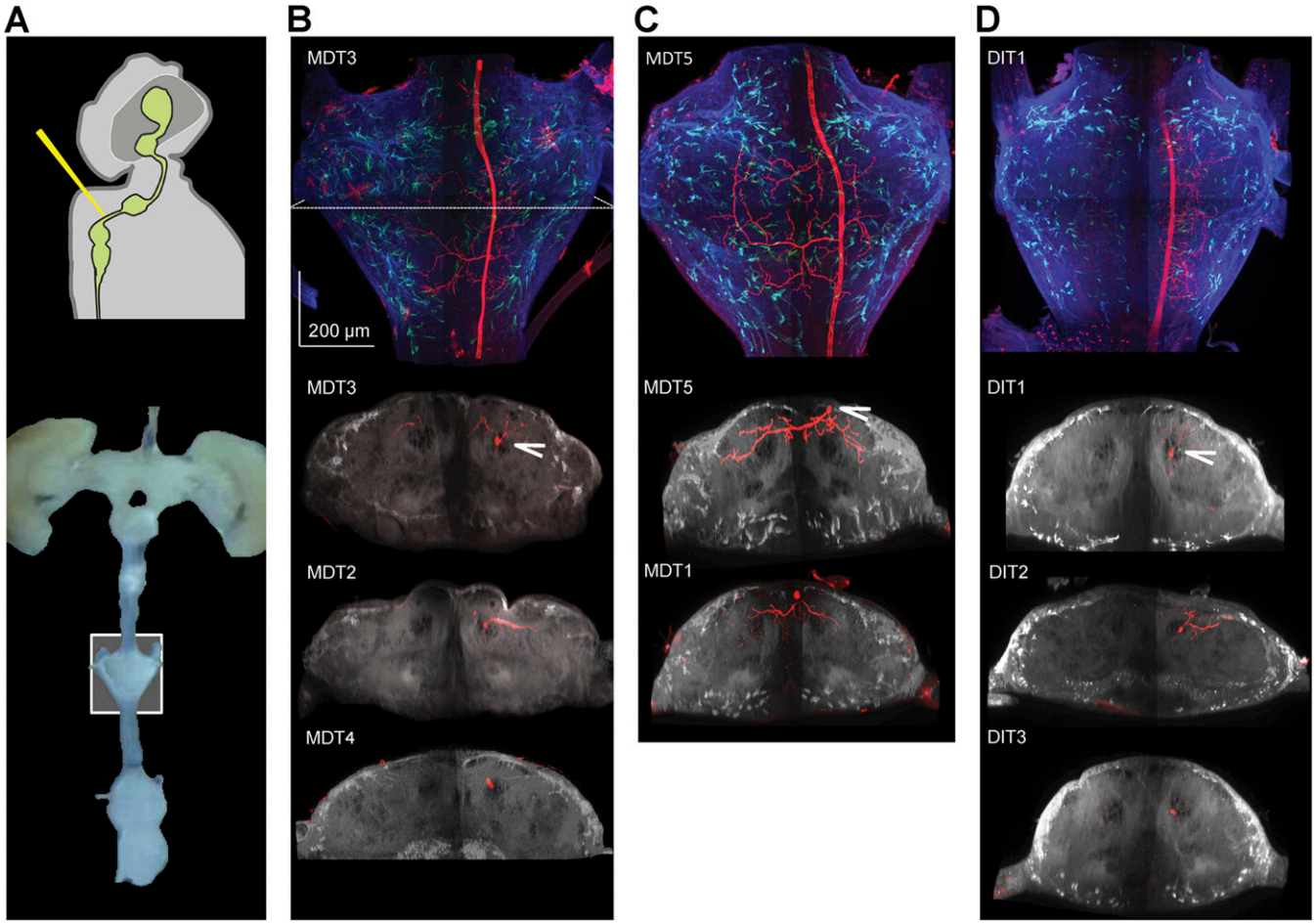

Fig. S7. In Libellulids, three TSDN types travel through a different track in the thoracic ganglia. (*A*) After injecting Lucifer yellow into the TSDN just above the mesothoracic ganglion, the central nervous system was dissected out and the ganglia imaged (prothoracic ganglion shown inside box). (*B–D*) (*Top*) Dorsal maximum-intensity projection showing TSDNs branching in the prothoracic ganglion. The eight middle and bottom panels show optical cross-sections through the prothoracic ganglion, each containing the fluorescence profile of a different TSDN type. Although we found homologous TSDNs between *L. luctuosa* and *A. junius*, we also found consistent differences between them. In the prothoracic ganglion of *L. luctuosa*, the axons of MDT3, MDT2, and MDT4 are found in the DIT track (*B*). Thus, MDT1 and MDT5 are the only two TSDNs found in the MDT track (*C*). All three DIT cells travel in the DIT track (*D*). The white arrows point at TSDN axons in cross-section. Due to the certainty of homology between Libellulid and Aeshnid TSDNs, and to avoid potential confusion in future comparisons, we followed the original naming system (1).

1. Olberg RM (1986) Identified target-selective visual interneurons descending from the dragonfly brain. *J Comp Physiol A Neuroethol Sens Neural Behav Physiol* 159(6):827–840.

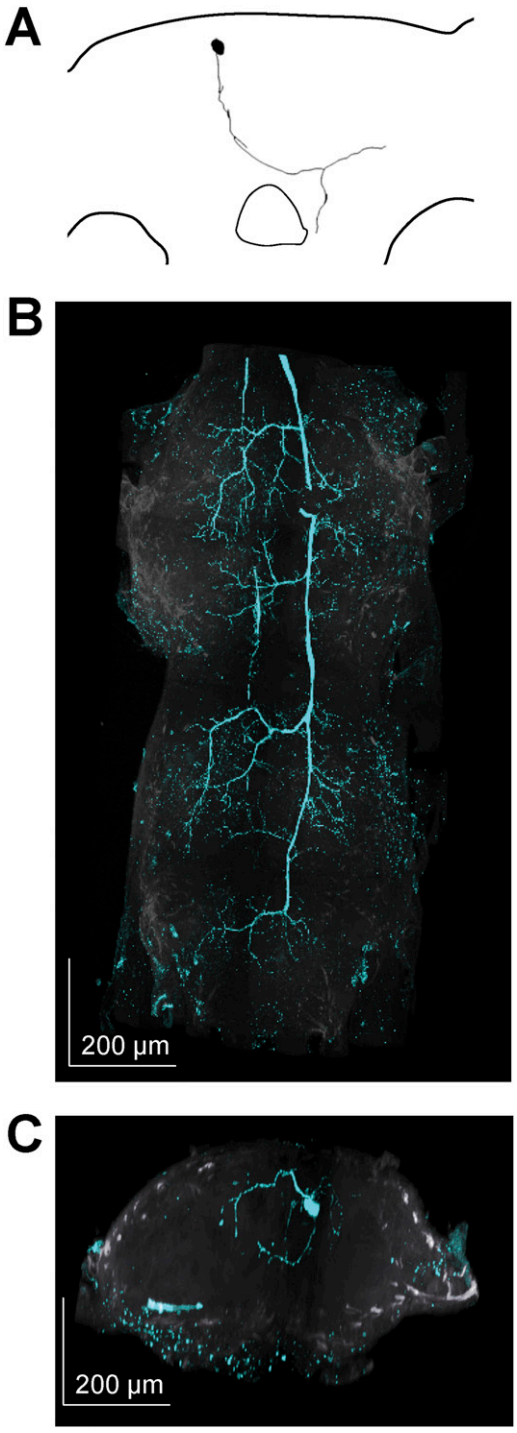

Fig. S8. MDT3 in the Libellulid *L. lydia* also travels through an alternative track. (*A*) Tracing of the brain fill showing the T shape characteristic of the MDT3 profile. (*B*) MIP projection of the neuron in the mesothoracic and metathoracic ganglia, showing the morphology typical of MDT3. (*C*) Cross-section of the prothoracic ganglion showing the axon traveling in the DIT track.

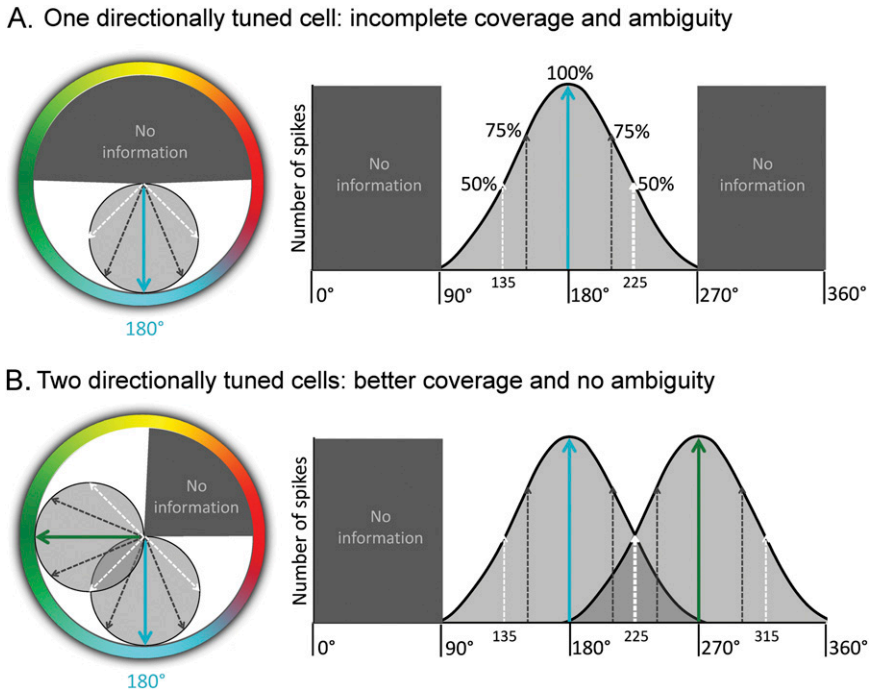

Fig. S9. Several cells are needed for a population vector to code equally well in all directions. The polar plots (*Left*) and linear plots (*Right*) both show the same information. (*A*) A single cell with a 45° tuning width does not provide full coverage for the detection of a target's direction (shown as areas of no information). In addition, only when the target travels in the preferred cell direction (100% cell activity, which equals to the maximum number of spikes) is the direction of the target coded without ambiguity. For every other direction covered by the tuning curve, the cell activity would code for two possible, opposing, directions. (*B*) Adding a second cell that displays a preferred direction shifted by 90°, decreases the number of directions where a target movement is not coded. In addition, ambiguity in the coding is now reduced. For example, both cells would need to spike at 50% of their maximum activity to code for a target moving with a 225° direction. If only cell 1 spikes at 50% and cell 2 remains silent, the target would be moving at 135°. The opposite ratio (cell 1 = 0%; cell 2 = 100%) would code for a target direction at 315°. Adding more cells would increase the ability of the system to code target direction more precisely.